Three-dimensional Structure of *Acanthamoeba castellanii* Myosin-IB (MIB) Determined by Cryoelectron Microscopy of Decorated Actin Filaments

James D. Jontes,* E. Michael Ostap,‡ Thomas D. Pollard,‡ and Ronald A. Milligan*

*Department of Cell Biology, The Scripps Research Institute, La Jolla, California 92037; and‡Department of Cell Biology and Anatomy, The Johns Hopkins University School of Medicine, Baltimore, Maryland 21205

Abstract. The *Acanthamoeba castellanii* myosin-Is were the first unconventional myosins to be discovered, and the myosin-I class has since been found to be one of the more diverse and abundant classes of the myosin superfamily. We used two-dimensional (2D) crystallization on phospholipid monolayers and negative stain electron microscopy to calculate a projection map of a "classical" myosin-I, *Acanthamoeba* myosin-IB (MIB), at ~18 Å resolution. Interpretation of the projection map suggests that the MIB molecules sit upright on the membrane. We also used cryoelectron microscopy and helical image analysis to determine the three-dimensional structure of actin filaments decorated with unphosphorylated (inactive) MIB. The catalytic domain is similar to that of other myosins, whereas the large carboxy-terminal tail domain differs greatly from brush border myosin-I (BBM-I), another member of the myosin-I class. These differences may be relevant to the distinct cellular functions of these two types of myosin-I. The catalytic domain of MIB also attaches to F-actin at a significantly different angle, ~10°, than BBM-I. Finally, there is evidence that the tails of adjacent MIB molecules interact in both the 2D crystal and in the decorated actin filaments.

THE myosin superfamily consists of at least 12 distinct classes that vary both in the sequence of their conserved myosin catalytic domains as well as in their unique tails (Mooseker and Cheney, 1995; Sellers and Goodson, 1995). For many years the only known myosins were the double-headed, filament-forming myosins found in muscle (conventional myosins or myosins-II). The remaining classes of myosin have been termed "unconventional myosins" to differentiate them from the myosins-II. Probably the most thoroughly studied class of unconventional myosins is the myosin-I class. These small, single-headed myosins bind to membrane lipids through a basic domain in their tail (for review see Pollard et al., 1991; Mooseker and Cheney, 1995). The first unconventional myosin (and first myosin-I) was isolated from *Acanthamoeba castellanii* (Pollard and Korn, 1973*a*,*b*), and was purified on the basis of its K^+, EDTA, and actin-activated MgATPase activities. However, this myosin was unusual in that it had a single heavy chain of ~140 kD, in contrast to the two ~200-kD heavy chains of myosin-II (Pollard and Korn, 1973*a*).

Three isoforms of the classical *Acanthamoeba* myosins-I are now known: myosins-IA, -IB, and -IC (Maruta and Korn, 1977*a*,*b*; Maruta et al., 1979). Each of the isoforms consists of a conserved myosin catalytic domain, a binding site for one or two light chains, a basic domain, a GPA[1](Q) domain (rich in glycine, proline and alanine [glutamine]), and an *scr*-homology domain-3 (SH3) domain (Pollard et al., 1991; Mooseker and Cheney, 1995). These myosins-I can associate with membranes or with actin filaments through their tail domains. An electrostatic association of myosin-I with anionic phospholipids and with base-stripped membranes has been shown to occur (Adams and Pollard, 1989; Miyata et al., 1989; Hayden et al., 1990), and this interaction has been mapped to the basic domain (Doberstein and Pollard, 1992). Interestingly, these myosins also contain a second, ATP-insensitive actin binding site (Lynch et al., 1986) enabling them to mediate actin–actin movements (Albanesi et al., 1985; Fujisaki et al., 1985). In myo-

J.D. Jontes's present address is Department of Molecular and Cellular Physiology, Stanford University School of Medicine, Stanford, CA 94305.

E.M. Ostap's present address is Department of Physiology, University of Pennsylvania School of Medicine, Philadelphia, PA 19104.

T.D. Pollard's present address is The Salk Institute for Biological Studies, La Jolla, CA 92037.

Address all correspondence to R.A. Milligan, Department of Cell Biology, MB25, The Scripps Research Institute, 10550 North Torrey Pines Road, La Jolla, CA 92037. Tel.: (619) 784-9827. Fax: (619) 784-2749. E-mail: milligan@scripps.edu

1. *Abbreviations used in this paper*: 2D, two-dimensional; 3D, three-dimensional; BBM-I, brush border myosin-I; GPA, glycine-proline-alanine; LCBD, light chain–binding domain; MIB, *Acanthamoeba* myosin-IB; SH3, *src*-homology domain-3.

sin-IA (Lynch et al., 1986) and myosin-IC (Doberstein and Pollard, 1992), this binding site was localized to the GPA domain.

Acanthamoeba myosins-I have maximal steady-state actin-activated ATPase rates of ~10–20 s^{-1} (Pollard and Korn, 1973*b*; Albanesi et al., 1983), and an unusual triphasic dependence upon actin concentration (Pollard and Korn, 1973*b*; Albanesi et al., 1983). This triphasic activation is due to the actin cross-linking ability imparted by the ATP-insensitive actin binding site on the tail (Albanesi et al., 1985). Analysis of the individual steps in the ATPase cycle by transient kinetics revealed that the mechanism of myosin-IA is similar to slow skeletal muscle myosin, whereas myosin-IB (MIB) is similar to fast skeletal muscle myosin (Ostap and Pollard, 1996). The in vitro motility of myosin-I has also been well characterized (Zot et al., 1992). The maximal rate of filament sliding is ~0.2 μm s^{-1}. Interestingly, this rate is ~10–50× slower than the rates observed for skeletal muscle myosin, even though the ATPase rates are comparable.

MIB consists of a 125-kD heavy chain and a single 27-kD light chain (Maruta et al., 1979; Jung et al., 1987). This isoform is primarily associated with the plasma membrane as well as vacuolar membranes (Baines et al., 1992). MIB appears to be associated with the plasma membrane at sites of phagocytosis and was concentrated at the tips of pseudopodia (Baines et al., 1992). This localization suggests that MIB may be involved in membrane dynamics at the cell surface. MIB is regulated by heavy chain phosphorylation of serine 411 (Brzeska et al., 1989, 1990), which is located at the actin-binding site (Rayment et al., 1993). Similar to the myosin-I isoforms in *Acanthamoeba*, heavy chain phosphorylation results in >20-fold activation of the actin-activated myosin-I ATPase activity (Albanesi et al., 1983). This activation is not the result of changes in the binding of myosin-I to F-actin (Albanesi et al., 1983; Ostap and Pollard, 1996). The transient kinetic studies of Ostap and Pollard (1996) suggest that phosphorylation regulates the rate-limiting phosphate release step, the transition from weakly bound intermediates in rapid equilibrium with actin to strongly bound states, capable of sustaining force.

Despite the extensive analysis of ameboid myosin-I biochemical properties and in vivo function, there is little structural information on these myosins. The only detailed structural information available for the myosins-I comes from recent electron microscopy studies on brush border myosin-I (BBM-I) (Jontes et al., 1995; Jontes and Milligan, 1997*a*,*b*; Whittaker and Milligan, 1997), a structurally distinct myosin-I subtype. Therefore, we investigated the structure of a "classical," ameboid-type myosin, *Acanthamoeba* MIB using electron microscopy. First, electron micrographs of negatively stained two-dimensional (2D) crystals were used to generate a projection map of MIB at ~18 Å resolution. In addition, we used cryoelectron microscopy and helical image analysis to produce a moderate resolution three-dimensional (3D) map (30 Å) of actin filaments decorated with MIB. These studies enabled us to compare the structure of MIB with BBM-I. The comparison of MIB with BBM-I reveals marked structural differences in the tail domains of these two proteins; MIB appears to have a much shorter "lever arm" and a more compact tail, whereas most of the BBM-I mass is composed of an extended light chain–binding domain (LCBD). In addition, the MIB catalytic domain appears to be slightly tilted compared to BBM-I, with respect to the F-actin axis. Our structural results suggest that these two types of myosin-I may have distinct intracellular functions.

Materials and Methods

Protein Preparation

MIB was prepared as described by Lynch et al. (1991). For 2D crystallization experiments, the MIB was frozen in 10-μl aliquots and then stored at −80°C until use. For cryo-EM experiments, the protein was maintained on ice and generally was used within a few days of thawing and within 2 wk of its preparation. Actin was prepared by the method of Spudich and Watt (1971).

2D Crystallization

MIB was diluted to 250 μg/ml in 10 mM Tris, pH 7.0, 13 mM NaCl, 1 mM $MgCl_2$, 1 mM EGTA, 1mM DTT, and 5% polyethylene glycol 10,000 (final concentrations). 15-μl drops were placed in 4 × 1 mm-teflon wells and then covered with 0.5–1.0 μl of 0.5 mg/ml 1,2-dioleoyl-sn-glycero-3-[phospho-L-serine] (Avanti Polar Lipids, Inc., Alabaster, AL), which had been diluted in chloroform. The protein solutions were incubated at room temperature for 8 h. Lipid films were adsorbed to carbon-coated copper grids by gently placing a grid carbon side down onto each well and then picking up the grid after 1–2 min. The grids were then negatively stained for 30–60 s in 2% uranyl acetate.

Electron Microscopy and Image Analysis of 2D Crystals

Images were collected in a transmission electron microscope (model CM12; Philips Electron Optics, Eindhoven, The Netherlands) operating at an accelerating voltage of 100 kV. Images were collected at a nominal 35,000× and at an underfocus of ~0.5 μm. Selected areas were scanned on a scanning microdensitometer (model 1010GM; Perkin-Elmer Corp., Norwalk, CT) using a spot and step size of 20 μm, corresponding to 5.71 Å at the specimen plane. Images were processed essentially as described in Jontes and Milligan (1997*a*). Lattice unbending was performed as described in Henderson et al. (1986). Only reflections present in three or more of the five images were used to calculate the projection map; this had the effect of truncating the data to a resolution of ~18 Å.

Preparation of Grids for Cryoelectron Microscopy

F-actin was diluted to ~20–40 μg/ml (~0.5–1.0 μM) in 10 mM Tris, pH 7.5, 100 mM KCl, 1 mM $MgCl_2$, 1 mM DTT, 1 mM EGTA, and then applied to electron microscopy grids covered with a holey carbon film. After ~2 min, the grids were washed with two drops of buffer and then myosin was applied to the grid at 1.0–1.5 mg/ml (6.5–10 μM). After another 2 min, the grids were blotted with filter paper and then plunged into ethane slush. Grids were stored under liquid nitrogen until use.

Cryoelectron Microscopy and Helical Image Analysis

Grids of actoMIB were mounted in a cryo stage (model 626; Gatan, Inc., Pleasanton, CA) and then inserted into a transmission electron microscope (model CM200; Philips Electron Optics) operating at an accelerating voltage of 100 kV. Images of filaments were taken under low-dose conditions at a nominal 38,000× and at an underfocus of ~1.5–2.0 μm.

Electron micrographs were screened in the optical diffractometer and then filaments were selected for scanning and computer processing. Images were required to be free of astigmatism and drift and to have appropriate levels of defocus. Selected images were then scanned using spot and step sizes of 25 μm, corresponding to 6.58 Å at the specimen. The PHOELIX software package (Whittaker et al., 1995; Carragher et al., 1996) was used for helical image processing performed essentially as described elsewhere (DeRosier and Moore, 1970; Whittaker et al., 1995). Steps included straightening of the filament axis, as well as correction for the contrast transfer function. Data were collected for Bessel orders ≤ 15 out to the 54th layer line (~27 Å).

The layer-line data from each filament were moved to a common phase origin and then averaged. One of the individual data sets was used as a

template for the initial round of fitting and averaging. The fitting and averaging procedure was iterated four times, with the averaged data set from the previous round acting as the new template for each successive round. The layer-line data from the final average was then used to "sniff" each individual data set (Morgan et al., 1995). The sniffed data were fit and averaged twice. The effect of sniffing on the strong layer lines was negligible but significantly improved the weaker layer lines by reducing scatter in the phases and boosting the amplitudes. The averaged layer-line data were truncated to 30 Å and were then used in a Fourier–Bessel synthesis to produce a 3D map. 26 layer lines were used to calculate the final map. Surface representations were made using the program SYNU (Hessler et al., 1992). Crystal structures were fit to the EM density using the program O (Jones et al., 1990).

Results

2D Crystals of MIB

MIB associates with monolayers of phosphatidylserine across a wide range of conditions (Doberstein and Pollard, 1992), but only small areas (~0.2–0.3 μm on edge) were ordered well enough for structural analysis (Fig. 1). These 2D crystals had *p*1 symmetry with lattice constants $a = b = 56.2 \pm 2.3$ Å, $\gamma = 119.0 \pm 1°$ and diffracted to ~18 Å resolution (Fig. 1 *b*). A projection map calculated from an average of five such images (average phase residual of 13.7 ± 3.8°) reveals a compact, globular asymmetric unit, ~56 Å × ~40 Å (Fig. 1 *d*). These globular densities are connected by a smaller density, a feature that is consistently present in each of the individual images. The strength of this connection suggests that mass from adjacent myosin molecules might be partially overlapping in projection. The low yield of well-ordered crystals prevented us from attempting a tilt series reconstruction of this protein, as was done for BBM-I (Jontes and Milligan, 1997*a*).

3D Map of MIB

Cryoelectron microscopy (Milligan and Flicker, 1987; Dubochet et al., 1988) of actin filaments decorated with purified *Acanthamoeba* MIB provided additional 3D information on MIB. Images of straightened actoMIB filaments (Fig. 2) tend to have a high background like BBM-I (Jontes and Milligan, 1997*b*). This may be due to a tendency of MIB to aggregate, even at KCl concentrations of 100 mM (Ostap, E.M., unpublished observations). 32 near or far sides from 17 filaments (4,239 actomyosin particles) were averaged to produce the layer-line data shown in Fig. 3. The mean phase residual for the fitting at the last iteration was 35.7°. The data were truncated to 30 Å and then used in a Fourier–Bessel synthesis to generate the 3D map (Fig. 4).

The 3D map of MIB has two distinguishable regions: a head, which contains the catalytic domain and LCBD, and a tail that presumably includes the lipid-binding domain,

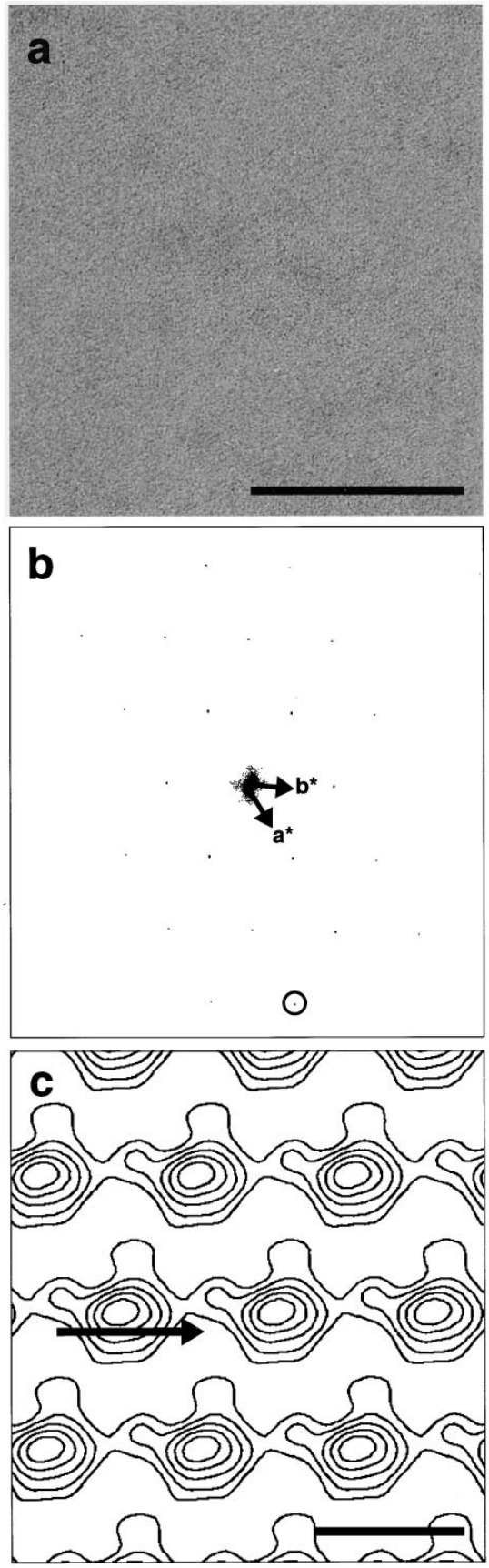

Figure 1. 2D crystals of MIB. (*a*) A high magnification electron micrograph of a negatively stained crystal of MIB. (*b*) The computed Fourier transform of the lattice-corrected image shown in *a*. The circled (*3*, *−1*) spot corresponds to a resolution of ~18 Å. (*c*) A *p*1 projection map calculated from the average of five individual images. The compact structure of the asymmetric unit suggests that the myosin is sitting upright on the lipid surface. The arrow indicates the presumed path of an unwound MIB helix, as discussed in the text. Bars: (*a*) 1,000 Å; (*c*) 50 Å.

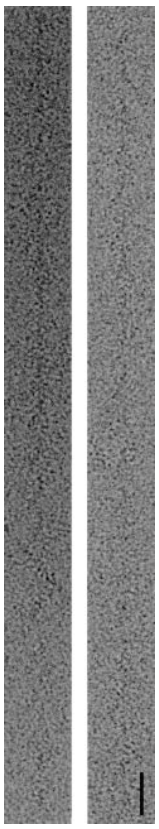

Figure 2. Actin filaments decorated with *Acanthamoeba* MIB. Cryoelectron micrographs of two computationally straightened actin filaments decorated with MIB. The presence of a high background makes it difficult to see the characteristic arrowhead pattern. Bar, 370 Å.

ATP-insensitive actin-binding site, and SH3 domain (Fig. 4 *b*). The globular catalytic domain binds tangentially to the actin filament in a manner similar to other myosins (Milligan and Flicker, 1987; Jontes et al., 1995; Whittaker et al., 1995). The massive MIB tail extends out from the filament axis for a short distance before angling sharply downward toward the barbed end of the filament (Fig. 4). Contacts between the tails of adjacent MIB molecules (Fig. 4) might be specific, although a gap may not be resolvable at 30 Å resolution.

Comparison of the MIB and BBM-I Tails

The map of MIB presented above allows a detailed structural comparison with BBM-I (Jontes et al., 1995; Jontes and Milligan, 1997*b*). Although both MIB and BBM-I are classified as myosins-I, they represent two distinct subtypes based on comparisons of catalytic domain sequences and of the organization of their divergent tail domains (Fig. 5; Mooseker and Cheney, 1995; Sellers and Goodson, 1995). The BBM-I tail consists of a single ~30-kD carboxy-terminal domain, characterized by a large proportion of basic amino acids. The MIB tail is more complex, having a GPA domain and an SH3 domain, in addition to the

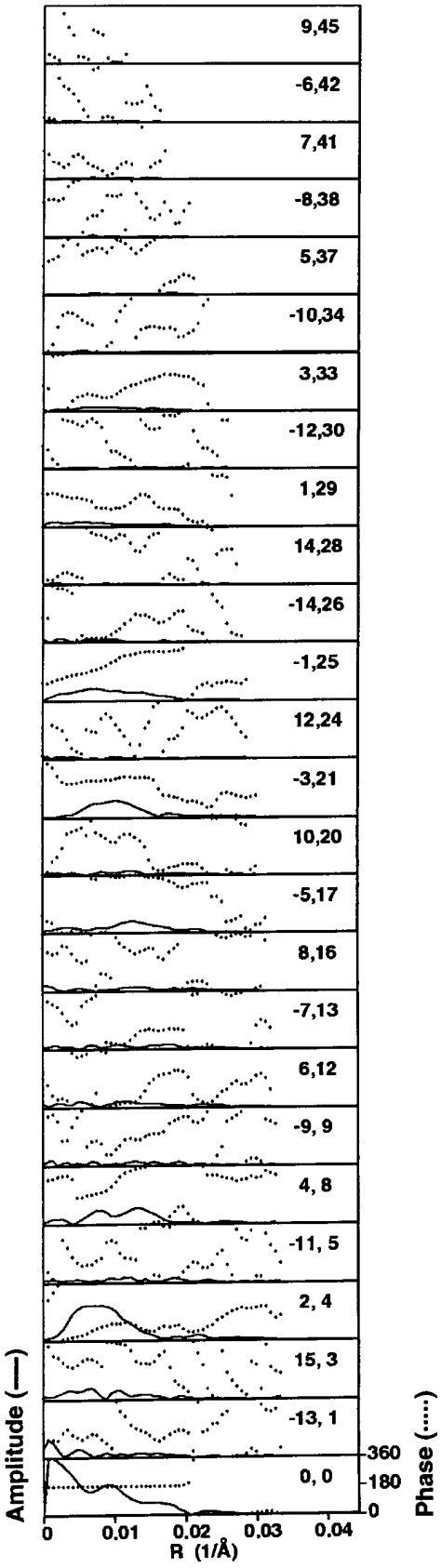

Figure 3. Averaged layer-line data set calculated from cryoelectron micrographs of actin filaments decorated with MIB. Data were obtained from the average of 32 near or far sides, representing 4,239 particles, and were truncated to 30 Å resolution. The ordered pairs of numbers (*n*, *1*) refer to the Bessel order and layer-line number, respectively, corresponding to a helical selection rule of 54 subunits in 25 turns.

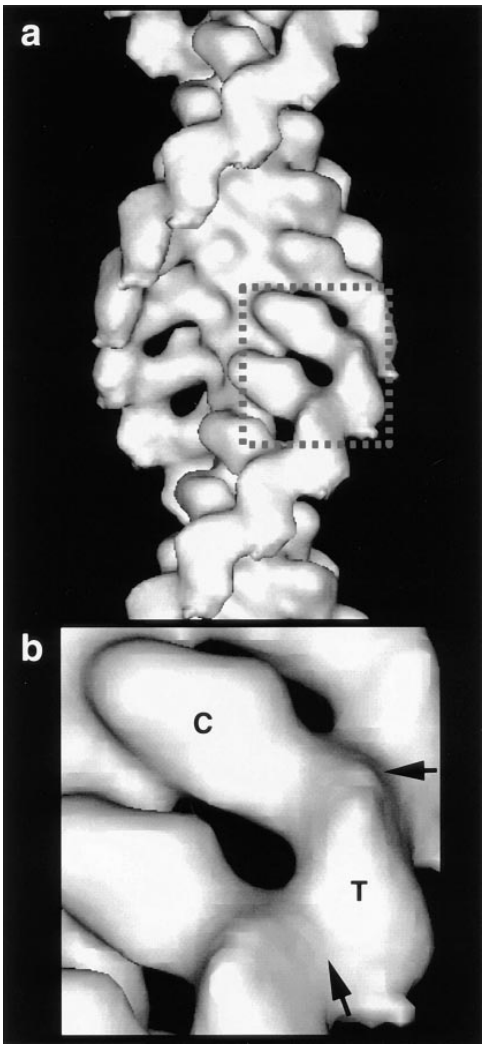

Figure 4. 3D map of MIB bound to actin. (*a*) The map looks similar to those obtained using the S1 portion of skeletal or smooth muscle myosins, due to the similar positions of the MIB tail and the S1 LCBD. (*b*) An enlarged view of the single myosin boxed off in *a. C*, catalytic domain; *T*, tail of the myosin. The arrows indicate contacts between the tails of successive myosins along the long-pitch actin helix. The surface of the map encloses ~100% of the expected MIB mass (~152 kD).

basic lipid–binding domain. The MIB tail is much more globular and compact than the BBM-I tail, which is a small and elongated density present just beyond the extended LCBD. Most of the mass of the MIB tail is also distal to the LCBD domain and must represent the lipid-binding region, the GPA domain, and the SH3 domain (Fig. 6).

Comparison of the MIB and BBM-I Heads

Although the tails exhibit substantial structural divergence, the motor domains of the two myosins-I are quite similar in shape (Fig. 6). To obtain a more objective comparison, the Cα backbone of the skeletal muscle myosin catalytic domain (Rayment et al., 1993) was fit into the EM maps to provide a visual assessment of the similarity of the molecular envelopes of MIB and BBM-I (Fig. 7). The crystal structure of the catalytic domain fits the 3D

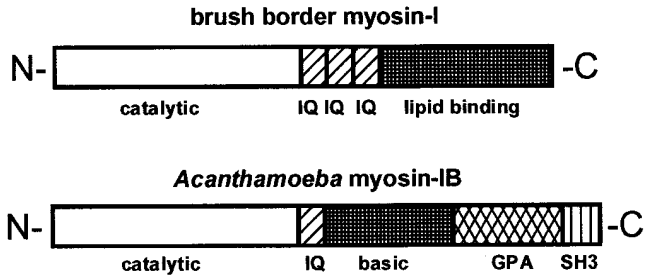

Figure 5. The domain organization of MIB and BBM-I (Hoshimaru and Nakanishi, 1987; Jung et al., 1987; Garcia et al., 1989).

map of MIB quite closely. The results of this modeling are qualitatively similar to those obtained for the fitting to BBM-I. This indicates that, to the resolution of our EM maps, the molecular envelopes of the MIB and BBM-I motor domains are indistinguishable, as expected from their sequence homology.

Although the molecular envelopes of the two myosin catalytic domains are very similar, they appear to interact with actin differently; the MIB is inclined at an angle relative to BBM-I (Fig. 6). In best fits (as determined by eye) of the X-ray structure to the two maps (Fig. 7), MIB is pivoted about the actin binding site by ~10° toward the barbed end of the actin. Whittaker and Milligan (1997) have previously demonstrated that BBM-I has an attachment to actin indistinguishable from that found for skeletal muscle myosin, indicating that the interaction of MIB with F-actin is distinct from both BBM-I and skeletal muscle subfragment-1.

The most prominent feature of the BBM-I molecule is the large, extended LCBD. The LCBD, with three associated calmodulin light chains, accounts for most of the visible mass beyond the BBM-I catalytic domain (Jontes and Milligan, 1997*a*,*b*). This part of the molecule projects out orthogonally from the filament axis, placing the lipid-binding domain at high radius (Jontes and Milligan, 1997*b*). The ~30 kD lipid-binding domain of BBM-I is the most

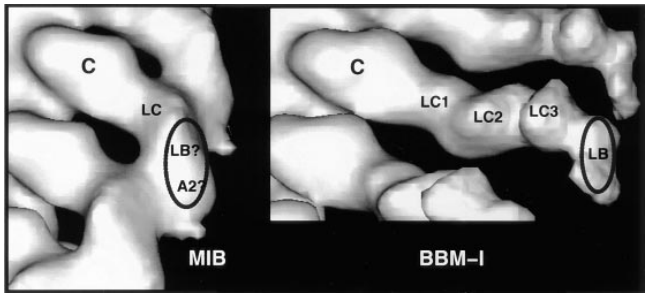

Figure 6. Comparison of the 3D maps of MIB and BBM-I. The catalytic domains (*C*) are very similar in overall shape, although they attach to actin at slightly different angles. BBM-I has an extended LCBD with three calmodulin light chains (LC1, -2, and -3), compared to the single light chain (*LC*) of MIB. MIB has a much larger tail, including a GPA and SH3 domain in addition to the basic, membrane-binding domain. Possible locations of the lipid-binding site (*LB?*) and secondary actin-binding site (*A2?*) are uncertain.

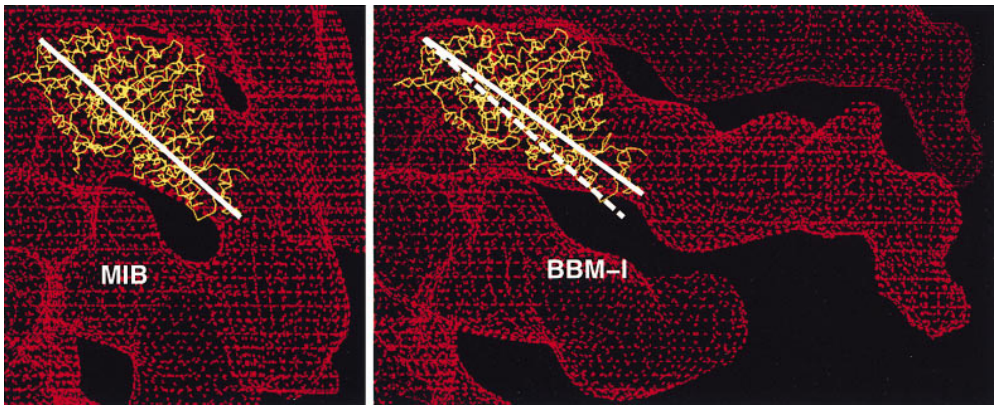

Figure 7. Fit of the atomic model of the skeletal muscle myosin catalytic domain into the EM envelopes of MIB and BBM-I. (*a*) The best fit, as determined by eye, of the Cα backbone of the skeletal muscle myosin S1 catalytic domain into the EM map of actoMIB. The solid white line is drawn through the catalytic domain to help compare the angle of attachment of MIB and BBM-I. (*b*) An identical view of BBM-I. The solid line represents a cord through the BBM-I catalytic domain and the dashed line is the cord drawn through the MIB catalytic domain shown in *a.* The molecular envelopes of the MIB and BBM-I catalytic domains are similar, but the angle of attachment to actin differs by ~10°.

distal density in the 3D map and extends to ~200 Å from the actin interface, ~80 Å further than MIB. The light chain–binding region of MIB consists of a single, 27-kD light chain bound to a lone IQ motif positioned just distal to the catalytic domain. This difference in the light chain-binding region constitutes one of the primary differences between the structures of these two myosins.

Discussion

The MIB Tail Domain

One of the most interesting aspects of the myosins-I is their interaction with plasma membranes. The myosins-I bind membranes in vitro (Adams and Pollard, 1989; Miyata et al., 1989; Hayden et al., 1990; Doberstein and Pollard, 1992) and are associated with membranes in vivo (Matsudaira and Burgess, 1979; Baines et al., 1992, 1995; Fath and Burgess, 1993; Fath et al., 1994). The MIB tail is particularly interesting due to its relative complexity compared to myosin-II, as well as to BBM-I. In addition to a putative lipid-binding site, it also has a second actin-binding site (allowing MIB to mediate actin–actin movements), as well as an SH3 domain. At 30 Å resolution, it is not possible to identify the distinct domains of the MIB tail, although it seems reasonable to suppose that the lipid binding site would be on the outer surface of the tail facing away from the actin (Fig. 6). In this orientation, MIB would assume a rather stubby appearance on the membrane (Fig. 8). This may result in significant geometric contraints placed upon the interaction of MIB with both membrane and actin. It has also been shown that membrane-bound MIB cannot also bind to actin through its ATP-insensitive actin-binding site (Miyata et al., 1989; Zot et al., 1992), suggesting that the secondary actin-binding site is also on the outer surface of the tail.

The rather compact LCBD and tail of MIB contrasts sharply with the long, extended structure of the BBM-I LCBD and tail (refer to Fig. 6). This structural difference may result in a markedly reduced working stroke for MIB compared with BBM-I or skeletal muscle myosin. The reduced size of the putative MIB lever arm may suggest that MIB moves as little as one-third the distance of BBM-I for each ATP hydrolyzed. This could explain the fact that the rates of in vitro motility for the ameboid myosins-I are much slower than would be expected based on their ATPase rates.

Jontes and Milligan (1997*a*,*b*) have suggested that the junction between the lipid-binding domain and the third calmodulin light chain might act like a hinge allowing BBM-I to pivot and interact with actin that approached the membrane from a range of angles and distances (Fig. 8). The much more massive junction in MIB makes it appear unlikely that MIB could have a similar degree of flexibility. This constraint could be reflected by the types of activities in which these two myosins-I are involved.

The strong connection between adjacent MIB tails at high radius in our 3D map (refer to Fig. 4), may represent a significant protein–protein interaction or simply may be an unresolved discontinuity. However, the projection map calculated from 2D crystals is consistent with this interaction being "real". First, the lattice constants of the crystal and the shape of the asymmetric unit indicate that the myosin must be sitting upright on the membrane with partial

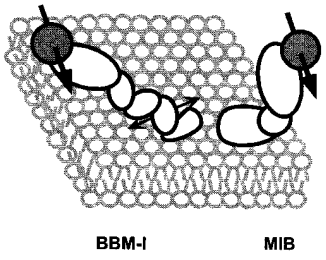

Figure 8. Diagram showing the interactions of MIB and BBM-I with membranes. The model highlights the very different structures of the two myosins-I. The BBM-I molecule (*left*) is elongated and binds to the membrane through a relatively small carboxy-terminal lipid-binding domain. The angle of BBM-I with respect to the membrane was determined from 2D crystals of BBM-I (Jontes and Milligan, 1997*a*). It has been suggested that the BBM-I should be flexible at the junction between the light chain-binding region and the lipid-binding domain (*double-headed arrow*). By contrast, the MIB molecule is compact, binding to the membrane through a centrally located lipid-binding region, which is part of a large, globular tail. *Shaded circles*, an actin monomer from an actin filament. The arrow shows the polarity of the filament, with the pointed end of the actin pointing out of the plane of the page.

superposition of adjacent molecules. Since the MIB tail is known to bind to phosphatidylserine, we assume that the tail is associated with the lipid monolayer and that the head points away from the membrane (Fig. 8). Given this orientation and the close packing of the molecules (refer to Fig. 1 *c*), it is likely that adjacent tails are in close contact. Furthermore, the spacing of 56 Å found in the planar crystal is very similar to the ~55 Å which would separate MIB molecules bound to successive subunits along the actin helix. Taken together, it is quite possible that the interaction observed in the helical map is also present in the 2D crystals. If this is the case, then the helical string of MIB molecules would have to "straighten out" to pack into the crystal (refer to Fig. 1 *c*). Given the kinetic evidence that MIB cannot work alone or in small numbers (Ostap and Pollard, 1996), this interaction between tails may contribute to the assembly of myosins-I into small functional groups, or "plaques". Consistent with this possibility, gold-labeled antibodies to MIB tended to cluster together on cellular membranes (Baines et al., 1992). Further studies will be required to determine whether or not MIB self-associates in vivo and what, if any, functional implications this might have.

Interaction of the MIB and BBM-I Catalytic Domains with F-Actin

Although the tails of MIB and BBM-I differ substantially, the catalytic domains appear very similar (refer to Figs. 6 and 7). Well-conserved proteins exhibiting similar structures at ~30 Å resolution is not surprising. In spite of the overall similarity in shape of the catalytic domains, we observe an intriguing difference in the angles of attachment to actin. The MIB molecule is inclined by ~10° at the actin-binding site relative to BBM-I (refer to Figs. 6 and 7). Interactions of the tails of adjacent myosins may contribute to this difference, although there is little evidence to suggest that a myosin bound in rigor would be flexible at the site of actin attachment (Cooke, 1981).

The absence of phosphorlyation of the MIB heavy chain may contribute to the difference in attachment. Phosphorylation of serine 411, located at the actin-binding site, activates the MIB enzymatic and motile activities (Brzeska et al., 1989; 1990). The MIB used in this study was unphosphorylated and, therefore, inactive. In contrast to the ameboid myosin-Is, most members of the myosin superfamily have an acidic residue at this site, the TEDS rule site, and can be considered to be constitutively phosphorylated and active (Bement and Mooseker, 1995; Mooseker and Cheney, 1995). If this idea is true, the attachment of phosphorylated MIB to actin may more closely resemble that of BBM-I. Alternatively, the altered interaction of MIB with actin might reflect a functional requirement unique to this myosin subclass. As mentioned above, the stubby appearance of MIB on the membrane may place geometric constraints on the interaction of MIB with actin, and then the altered attachment may represent a form of compensation or accommodation. It may also be worth noting that the actin used in this study (purified from rabbit back muscle) differs slightly from the actin with which either of these myosins would interact in vivo. Finally, the difference in angle of the attachment of MIB or BBM-I to actin might simply be due to an inherent difference between these two divergent motors, lacking any significant functional consequences.

Implications for Myosin-I Function

Structural and biochemical analysis of the *Acanthamoeba* myosin-Is and BBM-I have revealed major differences in the properties of these two types of myosin-I. Myosins-IA and -IB have kinetic properties very similar to those of the conventional myosins (Ostap and Pollard, 1996), having relatively robust rates of actin-activated ATP hydrolysis and spending a relatively short percentage of their cycles attached to actin. BBM-I, by contrast, has a very slow ATPase (Collins et al., 1990; Wolenski et al., 1993; Jontes et al., 1997) and may spend a longer time attached to actin (Jontes et al., 1997). Additionally, our structural results suggest that MIB likely has a much smaller working stroke than BBM-I, and that MIB may have the tendency to self-associate. Taken together, the evidence suggests that these myosins serve different subsets of cellular functions. Consistent with their kinetics and intracellular locations, the ameboid myosins-I may act as dynamic linkages in the cell periphery, forming contractile networks in the cell cortex and under the plasma membrane. These myosins-I would function as a cellular population and would be able to modulate and coordinate many cell surface activities such as exocytosis, endocytosis, cell migration, and pseudopod and filopodial extension (Jung et al., 1993, 1996; Novak et al., 1995; Novak and Titus, 1997). The BBM-I type of myosin-I would be better suited to motile activites where they worked in smaller numbers, such as transporting vesicles (Drenkhahn and Dermietzel, 1988; Fath and Burgess, 1993; Fath et al., 1994) or acting as an adaptation motor (Assad and Corey, 1992; Hudspeth and Gillespie, 1993). Thus, analysis of the biochemical and structural properties of unconventional myosins may help to focus investigation into their cellular functions.

J.D. Jontes would like to thank B. Carragher (Beckman Institute, University of Illinois, Urbana-Champaign, IL) for access to the Philips CM200TEM and for her hospitality during collection of the MIB helical data.

This work was supported by research grants from the National Institutes of Health (Bethesda, MD) to R.A. Milligan (AR-39155), and to T.D. Pollard (GM-26132). E.M. Ostap was supported in part by a grant from the Cancer Research Fund of the Damon Runyon–Walter Winchell Foundation Fellowship (DRG-1294). J.D. Jontes was supported by a predoctoral fellowship from the Howard Hughes Medical Institute (Chevy Chase, MD).

Received for publication 14 November 1997 and in revised form 26 January 1998.

References

Adams, R.J., and T.D. Pollard. 1989. Binding of myosin I to membrane lipids. *Nature.* 340:565–568.

Albanesi, J.P., J.A. Hammer III, and E.D. Korn. 1983. The interaction of f-actin with phosphorylated and unphosphorylated myosins IA and IB from *Acanthamoeba castellanii. J. Biol. Chem.* 258:10176–10181.

Albanesi, J.P., H. Fujisaki, and E.D. Korn. 1985. A kinetic model for the molecular basis of contractile activity of *Acanthamoeba* myosins IA and IB. *J. Biol. Chem.* 260:11174–11179.

Assad, J.A., and D.P. Corey. 1992. An active motor model for adaptation by vertebrate hair cells. *J. Neurosci.* 12:3291–3309.

Baines, I.C., H. Brzeska, and E.D. Korn. 1992. Differential localization of *Acanthamoeba* myosin I isoforms. *J. Cell Biol.* 119:1193–1203.

Baines, I.C., A. Corigliano-Murphy, and E.D. Korn. 1995. Quantification and localization of phosphorylated myosin I isoforms in *Acanthamoeba castellanii. J. Cell Biol.* 130:591–603.

Bement, W.M., and M.S. Mooseker. 1995. TEDS rule: a molecular rationale for differential regulation of myosins by phosphorylation of the heavy chain head. *Cell Motil. Cytoskel.* 31:87–92.

Brzeska, H., T.J. Lynch, B. Martin, and E.D. Korn. 1989. The localization and sequence of the phosphorylation sites of *Acanthamoeba* myosins-I. *J. Biol. Chem.* 264:19340–19348.

Brzeska, H., T.J. Lynch, B. Martin, A. Corigliano-Murphy, and E.D. Korn. 1990. Substrate specificity of *Acanthamoeba* myosin-I heavy chain kinase as determined with synthetic peptides. *J. Biol. Chem.* 265:16138–16144.

Carragher, B.O., M. Whittaker, and R.A. Milligan. 1996. Helical processing using PHOELIX. *J. Struct. Biol.* 116:107–112.

Collins, K., J.R. Sellers, and P. Matsudaira. 1990. Calmodulin dissociation regulates brush border myosin I (110-kD–calmodulin) mechanochemical activity in vitro. *J. Cell Biol.* 110:1137–1147.

Cooke, R. 1981. Stress does not alter the conformation of a domain of the myosin cross-bridge in rigor muscle fibres. *Nature.* 294:570–571.

DeRosier, D.J., and P.B. Moore. 1970. Reconstruction of three-dimensional images from electron micrographs of structures with helical symmetry. *J. Mol. Biol.* 52:355–369.

Doberstein, S.K., and T.D. Pollard. 1992. Localization and specificity of the phospholipid and actin binding sites on the tail of *Acanthamoeba* myosin IC. *J. Cell Biol.* 117:1241–1249.

Drenkhahn, D., and R. Dermietzel. 1988. Organization of the actin filament cytoskeleton in the intestinal brush border: a quantitative and qualitative immunoelectron microscope study. *J. Cell Biol.* 107:1037–1048.

Dubochet, J., M. Adrian, J.-J. Chang, J.-C. Homo, J. Lepault, A.W. McDowall, and P. Schultz. 1988. Cryo-electron microscopy of vitrified specimens. *Q. Rev. Biophys.* 21:129–228.

Fath, K.R., and D.R. Burgess. 1993. Golgi-derived vesicles from developing epithelial cells bind actin filaments and possess myosin-I as a cytoplasmically-oriented peripheral membrane protein. *J. Cell Biol.* 120:117–127.

Fath, K.R., G.M. Trimbur, and D.R. Burgess. 1994. Molecular motors are differentially distributed on Golgi membranes from polarized epithelial cells. *J. Cell Biol.* 126:661–675.

Fujisaki, H., J.P. Albanesi, and E.D. Korn. 1985. Experimental evidence for the contractile activities of *Acanthamoeba* myosins IA and IB. *J. Biol. Chem.* 260:11183–11189.

Garcia, A., E. Coudrier, J. Carboni, J. Anderson, J. Vandekerckhove, M. Mooseker, D. Louvard, and M. Arpin. 1989. Partial deduced sequence of the 110-kD–calmodulin complex of the avian intestinal microvillus shows that this mechano enzyme is a member of the myosin I family. *J. Cell Biol.* 109: 2895–2903.

Hayden, S.M., J.S. Wolenski, and M.S. Mooseker. 1990. Binding of brush border myosin I to phospholipid vesicles. *J. Cell Biol.* 111:443–451.

Henderson, R., J.M. Baldwin, K.H. Downing, J. Lepault, and F. Zemlin. 1986. Structure of purple membrane from *Halobacterium halobium*: recording, measurement and evaluation of electron micrographs at 3.5 Å resolution. *Ultramicroscopy.* 19:147–178.

Hessler, D., S.J. Young, B.O. Carragher, M. Martone, J.E. Hinshaw, R.A. Milligan, E. Masliah, M. Whittaker, S. Lamont, and M.H. Ellisman. 1992. SYNU: Software for Visualization of 3-Dimensional Biological Structures. *In* Microscopy: The Key Research Tool (C.E. Lyman, L.D. Peachey, and R.M. Fisher, editors.) EMSA Inc., Milwaukee, WI. 73–82.

Hoshimaru, M., and S. Nakanishi. 1987. Identification of a new type of mammalian myosin heavy chain by molecular cloning. Overlap of its mRNA with prepro tachykinin B mRNA. *J. Biol. Chem.* 262:14625–14632.

Hudspeth, A.J., and P. Gillespie. 1994. Pulling springs to tune transduction: adaptation by hair cells. *Neuron.* 12:1–9.

Jones, T.A., J.Y. Zou, S.W. Cowan, and M. Kjeldgaard. 1991. Improved methods for building protein models in electron density maps and the location of errors in these models. *Acta Crystallogr.* A47:110–119.

Jontes, J.D., E.M. Wilson-Kubalek, and R.A. Milligan. 1995. A 32° tail swing in brush border myosin I on ADP release. *Nature.* 378:751–753.

Jontes, J.D., and R.A. Milligan. 1997*a.* Three-dimensional structure of brush border myosin-I at ~20Å resolution by electron microscopy and image analysis. *J. Mol. Biol.* 266:331–342.

Jontes, J.D., and R.A. Milligan. 1997*b.* Brush border myosin-I structure and ADP-dependent conformational changes revealed by cryoelectron microscopy and image analysis. *J. Cell Biol.* 139:683–693.

Jontes, J.D., R.A. Milligan, T.D. Pollard, and E.M. Ostap. 1997. Kinetic characterization of the brush border myosin-I ATPase. *Proc. Natl. Acad. Sci. USA.* 94:14332–14337.

Jung, G., E.D. Korn, and J.A. Hammer III. 1987. The heavy chain of *Acanthamoeba* myosin IB is a fusion of myosin-like and non-myosin-like sequences. *Proc. Natl. Acad. Sci. USA.* 84:6720–6724.

Jung, G., Y. Fukui, B. Martin, and J.A. Hammer III. 1993. Sequence, expression pattern, intracellular localization, and targeted disruption of the *Dictyostelium* myosin ID heavy chain isoform. *J. Biol. Chem.* 268:14981–14990.

Jung, G., X. Wu, and J.A. Hammer III. 1996. *Dictyostelium* mutants lacking multiple classic myosin I isoforms reveal combinations of shared and distinct functions. *J. Cell Biol.* 133:305–323.

Lynch, T.J., J.P. Albanesi, E.D. Korn, E.A. Robinson, B. Bowers, and H. Fujisaki. 1986. ATPase activities and actin-binding properties of subfragments of *Acanthamoeba* myosin IA. *J. Biol. Chem.* 261:17156–17162.

Lynch, T.J., H. Brzeska, I.C. Baines, and E.D. Korn. 1991. Purification of myosin-I and myosin-I heavy chain kinase for *Acanthamoeba castellanii. Methods Enzymol.* 196:12–23.

Maruta, H., and E.D. Korn. 1977*a.* Purification from *Acanthamoeba castellanii* of proteins that include gelation and syneresis of F-actin. *J. Biol. Chem.* 252: 399–402.

Maruta, H., and E.D. Korn. 1977*b. Acanthamoeba* myosin II. *J. Biol. Chem.* 252:6501–6509.

Maruta, H., H. Gadasi, J.H. Collins, and E.D. Korn. 1979. Multiple forms of *Acanthamoeba* myosin I. *J. Biol. Chem.* 254:3624–3630.

Matsudaira, P.T., and D.R. Burgess. 1979. Identification and organization of the components in the isolated microvillus cytoskeleton. *J. Cell Biol.* 83:667–673.

Milligan, R.A., and P. Flicker. 1987. Structural relationships of actin, myosin and tropomyosin revealed by cryoelectron microscopy. *J. Cell Biol.* 105:29–39.

Miyata, H., B. Bowers, and E.D. Korn. 1989. Plasma membrane association of *Acanthamoeba* myosin I. *J. Cell Biol.* 109:1519–1528.

Mooseker, M.S., and R.E. Cheney. 1995. Unconventional myosins. *Annu. Rev. Cell Dev. Biol.* 11:633–675.

Morgan, D.G., C. Owen, L.A. Melanson, and D.J. DeRosier. 1995. Structure of bacterial flagellar filaments at 11 Å resolution: packing of the alpha helices. *J. Mol. Biol.* 249:88–110.

Novak, K.D., and M.A. Titus. 1997. Myosin I overexpression impairs cell migration. *J. Cell Biol.* 136:633–647.

Novak, K.D., M.D. Peterson, M.C. Reedy, and M.A. Titus. 1995. *Dictyostelium* myosin I double mutants exhibit conditional defects in pinocytosis. *J. Cell Biol.* 131:1205–1221.

Ostap, E.M., and T.D. Pollard. 1996. Biochemical kinetic characterization of the *Acanthamoeba* myosin-I ATPase. *J. Cell Biol.* 132:1053–1060.

Pollard, T.D., and E.D. Korn. 1973*a. Acanthamoeba* myosin. I. Isolation from *Acanthamoeba castellanii* of an enzyme similar to muscle myosin. *J. Biol. Chem.* 248:4682–4690.

Pollard, T.D., and E.D. Korn. 1973*b. Acanthamoeba* myosin. II. Interaction with actin and with a new cofactor protein required for actin activation of Mg^{2+} adenosine triphosphatase activity. *J. Biol. Chem.* 248:4691–4697.

Pollard, T.D., S.K. Doberstein, and H.G. Zot. 1991. Myosin-I. *Annu. Rev. Physiol.* 53:653–681.

Rayment, I., W.R. Rypniewski, K. Schmidt-Base, R. Smith, D.R. Tomchick, M.M. Benning, D.A. Winkelmann, G. Wesenberg, and H.M. Holden. 1993. Three-dimensional structure of myosin subfragment-1: a molecular motor. *Science.* 261:50–58.

Sellers, J.R., and H.V. Goodson. 1995. Motor proteins 2: myosin. *Protein Profile.* 2(12).

Spudich, J.A., and S. Watt. 1971. The regulation of rabbit skeletal muscle contraction. *J. Biol. Chem.* 246:4866–4871.

Whittaker, M., and R.A. Milligan. 1997. Conformational changes due to calcium-induced calmodulin dissociation in brush border myosin I-decorated F-actin revealed by cyoelectron microscopy and image analysis. *J. Mol. Biol.* 269:548–557.

Whittaker, M., B.O. Carragher, and R.A. Milligan. 1995. PHOELIX: a package for semi-automated helical reconstruction. *Ultramicroscopy.* 58:245–259.

Wolenski, J.S., S.M. Hayden, P. Forscher, and M.S. Mooseker. 1993. Calcium–calmodulin and regulation of brush border myosin-I MgATPase and mechanochemistry. *J. Cell Biol.* 122:613–621.

Zot, H.G., S.K. Doberstein, and T.D. Pollard. 1992. Myosin–I moves actin filaments on a phospholipid substrate: implications for membrane targeting. *J. Cell Biol.* 116:367–376.